Anagnostou, E.*[a,b], Williams, B.[c], Westfield, I.[a], Foster, G.L.[b], Ries, J.B.[a]

[a] Northeastern University, Marine Science Center, 430 Nahant Road, Nahant, MA 01908, USA

[b] GEOMAR Helmholtz Centre for Ocean Research Kiel, Germany

[c] W.M. Keck Science Department, Claremont McKenna College, Pitzer College, Scripps College, 925 N Mills Ave, Claremont CA, 91711 USA

[d] Ocean and Earth Science, University of Southampton, European Way, Southampton, SO14 3ZH, UK

*corresponding author: eanagnostou@geomar.de

Calibration of the pH-$\delta^{11}B$ and temperature-Mg/Li proxies in the long-lived high-latitude crustose coralline red alga *Clathromorphum compactum* via controlled laboratory experiments

Abstract

A solid understanding of global oceanic change throughout Holocene time is needed to contextualize and interpret recent observations of rapid warming (Moore, 2016), ocean acidification (Popova et al., 2014; Qi et al., 2017), increasing meltwater input (Halfar et al., 2013; Notz and Stroeve, 2016) and circulation changes (Liu et al., 2017; Rahmstorf et al., 2015; Yang et al., 2016) in the Arctic and subarctic Oceans. Precisely reconstructing acidification and temperature variations throughout the Holocene will provide a vital context for interpreting current environmental changes and future climate projections in the region. However, existing paleoenvironmental reconstructions are sparse and uncertain, largely owing to limited availability of high fidelity paleoceanographic archives, such as marine carbonates, in high latitude waters. Coralline algae of the genus *Clathromorphum* have emerged as key candidates for reconstructing high-latitude environmental variability at annual to sub-annual resolution. Here, we present the first empirical calibrations of boron isotope-pH and Mg/Li-temperature relationships within the long-lived, crustose coralline red alga *Clathromorphum compactum*. Calibration experiments were performed in triplicate, growing wild-collected specimens for four months at three controlled temperatures (6.4 – 12.4 ^{o}C) and four pCO_2 conditions (352 - 3230 ppm), to test the effects of these environmental parameters on the isotopic and elemental composition of the algal skeleton. We find that boron isotopes within the skeleton of *C. compactum* ($\delta^{11}B_{cc}$) are well correlated with $\delta^{11}B$ of seawater borate ($\delta^{11}B_{borate}$), defining the following equation: $\delta^{11}B_{cc}$ (2σ) = 1.46 (0.06) $\delta^{11}B_{borate}$ + 6.91 (0.72). This equation can be used to reconstruct $\delta^{11}B_{borate}$ of the coralline alga's ambient seawater, from which past seawater pH can be calculated. We also identified a strong correlation between skeletal Mg/Li ratio and seawater temperature,

defined by the equation: Mg/Li (2σ) = 0.17 (0.02) temperature (^{o}C) + 1.02 (0.16). Therefore, despite the strong biological control that this species appears to exert on calcification site pH (elevated 1.0-1.6 pH units above seawater pH, inferred from $\delta^{11}B_{cc} > \delta^{11}B_{borate}$), and the apparent relationship between skeletal extension rate and skeletal Li/Ca and Mg/Ca, the $\delta^{11}B_{cc}$ and Mg/Li ratios of the coralline alga's skeleton strongly and significantly respond to ambient seawater pH and temperature, respectively. These results support the use of $\delta^{11}B$ and Mg/Li within *C. compactum* for pH and temperature reconstructions of northern high-latitude oceans.

1.0 Introduction

1.1 Coralline algae as paleoenvironmental archives

Recent observations of dramatic warming (Moore, 2016), acidification (Popova et al., 2014; Qi et al., 2017), increasing meltwater input (Halfar et al., 2013; Notz and Stroeve, 2016), and circulation changes (Liu et al., 2017; Rahmstorf et al., 2015; Yang et al., 2016) in the Arctic and subarctic oceans suggest that these regions are particularly sensitive to impacts of anthropogenic global change. However, a better understanding of pre-anthropogenic environmental variations throughout Holocene time is needed to contextualize and interpret these changes, and to inform predictions of future change. Existing paleoceanographic reconstructions for these regions are relatively sparse and highly uncertain, largely because of the limited availability of reliable paleoceanographic archives in high-latitude waters, such as annually layered marine carbonates.

Crustose coralline red algae have been used for paleoecological reconstructions of geological intervals dating back to the early Tertiary (Adey, 1979). However, they have only recently been used to reconstruct environmental change of the Common Era (Burdett et al., 2011; Chan et al., 2011; Fietzke et al., 2015; Halfar et al., 2011; Hetzinger et al., 2018; Hetzinger et al., 2009; Kamenos, 2012; Kamenos and Law, 2010; Williams et al., 2011). This was largely because of incomplete understanding of the coralline algae's complex anatomy and the lack of suitable methodologies for analysing geochemical signals within their skeletons with the required spatial resolution and analytical accuracy. Coralline algae of the genus *Clathromorphum* have emerged as a promising climate archive of high-latitude marine environments, because of their resolvable annual growth bands and multi-century lifespan (Frantz et al., 2005; Halfar et al., 2013; Halfar et al., 2007), and their wide distribution in mid- and high-latitude environments throughout the northwest Atlantic, North Pacific, and

Arctic Oceans (Adey et al., 2008) (Figure 1). This has led to increased assessment of the genus's climate archiving potential.

1.2 Ecology of coralline algae

Coralline algae are the most diverse and abundant calcareous organisms within intertidal and shallow subtidal zones around the world (Steneck, 1986). They are keystone species within such ecosystems because they provide substrate for larval settlement of invertebrates onto rocky and sediment-dominated substrates. They also provide food for grazers, function as nursery grounds for a number of species (Chenelot et al., 2011; Steneck and Martone, 2007), and increase the structural integrity of reefs and sediments within the photic zone (Heyward and Negri, 1999; Roberts, 2001). Depending on their degree of control over calcification, dissolution, and grazing of their relatively soluble high-Mg calcite skeleton, ocean acidification and warming may have highly deleterious effects on their growth and survival (Borowitzka and Larkum, 1987; Fabricius et al., 2015; Hoegh-Guldberg et al., 2007; Ries et al., 2009). Specifically, coralline algae in colder, higher-latitude waters, which are characterized by lower calcium carbonate saturation states owing to increased solubility of atmospheric CO_2 and increasing meltwater input, could reach their limits of resilience even sooner than species of coralline algae in warmer, low latitude locations.

1.3 Calcification within Clathromorphum *coralline algae*

Coralline algae of the genus *Clathromorphum* grow at a rate of 300-400 μm yr^{-1} in the warmer fringes of the subarctic ocean and Aleutian Islands, and 100 μm yr^{-1} or less in the colder reaches of the subarctic and Arctic oceans (Adey et al., 2013). *Clathromorphum* produce annually resolved layers of high Mg-calcite crystals over their lifetime, delineated by seasonal changes in skeletal density (Chan et al., 2017). Living tissue and photosynthetic epithelial cells cover the meristem, protecting the calcified layers beneath the meristem, the perithallium, from diagenetic alteration (Alexandersson, 1974) and from herbivory (Steneck, 1986). A continuous record of skeletal accretion is thereby maintained in the perithallium (Adey et al., 2013; Steneck, 1982), which is well-suited for archiving high-resolution paleoenvironmental variability (Figure 2). This mode of calcification contrasts that of other species of coralline algae that lack the meristem, and instead calcify across several cell layers below the coralline alga's surface, creating a diffusive, time-integrated band of calcification (Adey et al., 2013), limiting the temporal resolution of the archive.

Calcification within coralline algae is likely regulated by a number of metabolic processes that influence the carbonate system, including photosynthesis and respiration (Beer and Larkum, 2001; Gao et al., 1993; Hurd et al., 2011; Martin et al., 2013; Smith and Roth, 1979). For example, the calcification rate of coralline algae has been directly linked to photosynthetic rate (Pentecost, 1978) and the availability of dissolved inorganic carbon (Digby, 1977; Gao et al., 1993). Seawater dissolved inorganic carbon is converted to CO_2 for photosynthesis within the algae through the action of the enzyme carbonic anhydrase, ion transporters, and proton pumps (Comeau et al., 2013; Hofmann et al., 2016; McConnaughey and Falk, 1991; McConnaughey and Whelan, 1997). Photosynthesis, in turn, removes CO_2, thereby increasing local calcite saturation state and promoting calcification (Gao et al., 1993). Calcein staining and boron isotope studies indicate that, for some species of coralline algae, the site of calcification is partially open to seawater exchange (Donald et al., 2017; Pauly et al., 2015), even though calcification also occurs extracellularly in *Clathromorphum*, in a region bound by the walls of adjacent cells (Adey et al., 2013). The role of photosynthesis in coralline algal calcification is unclear in the genus *Clathromorphum*, as they calcify even under extended periods of darkness (Adey, 1998; Adey et al., 2013). This may arise from the algae's ability to store energy during periods of ample light and photosynthesis (Adey et al., 2013), and supports prior assertions that organic templates and ion pumps are also important in coralline algal calcification (Adey, 1998; Borowitzka and Larkum, 1987; Rahman and Halfar, 2014).

1.4 Boron isotope systematics

Boron isotopes in several marine carbonates have been used as a proxy of paleo-seawater pH (Foster and Rae, 2016; Hemming and Hanson, 1992; Zeebe and Wolf-Gladrow, 2001). The basis for the boron isotope proxy of seawater pH stems from the observation that both the borate abundance and the boron isotopic composition of borate in seawater ($\delta^{11}B_{borate}$) increases systematically with increasing seawater pH (Zeebe and Wolf-Gladrow, 2001). The relationship between $\delta^{11}B_{borate}$ and seawater pH (pH_{sw}) is described as follows:

$$pH_{sw} = pK^*_B - \log\left[-\frac{\delta^{11}B_{sw} - \delta^{11}B_{borate}}{\delta^{11}B_{sw} - (\alpha_B \delta^{11}B_{borate} - 1000(\alpha_B - 1))}\right] \quad (1)$$

where pK^*_B is the constant describing the dissociation equilibrium between boric acid and borate ion in seawater (Dickson, 1990a), $\delta^{11}B_{sw}$ is the seawater boron isotopic composition (in delta notation relative to NIST SRM 951 boric acid), and α_B is the equilibrium constant

for boron isotope fractionation between boric acid and borate ion in seawater (1.0272; (Klochko et al., 2006) within uncertainty of other estimates (Nir et al., 2015)).

Many species of calcium carbonate precipitating organisms elevate their calcifying fluid pH (pH_{cf}) to promote calcification, as revealed by pH-microelectrode, pH-sensitive dyes, and/or boron isotope studies (Al-Horani et al., 2003; Anagnostou et al., 2012; Holcomb et al., 2014; Krief et al., 2010; McCulloch et al., 2012; Ries, 2011; Sutton et al., 2018; Venn et al., 2011; Venn et al., 2013). Therefore, to estimate pH_{sw} from skeletal $\delta^{11}B$ ($\delta^{11}B_{cc}$) of coralline algal calcite, which prior studies suggest occurs primarily as borate ion, (Cornwall et al., 2017; Donald et al., 2017), species-specific relationships must be empirically defined between seawater $\delta^{11}B_{borate}$ and $\delta^{11}B_{cc}$. These relationships are used to convert $\delta^{11}B_{cc}$ into $\delta^{11}B_{borate}$, which can then be substituted into equation (1) to solve for pH_{sw}.

1.5 pH and temperature proxies in coralline algae

There is no established calibration of the $\delta^{11}B_{cc}$ vs. pH_{sw} proxy in any species of coralline red alga. However, coralline algal $\delta^{11}B$ has been used to estimate pH at the alga's site of calcification. For example, $\delta^{11}B_{cc}$ was found to be substantially elevated relative to $\delta^{11}B_{borate}$ of the ambient seawater in two species of low-latitude branching, non-articulate coralline algae (*Neogoniolithon* sp. and *Sporolithon durun*) and within one species of low-latitude articulate coralline red alga (*Amphiroa anceps*) cultured over a range of controlled pCO_2 conditions. The increase in $\delta^{11}B_{cc}$ relative to $\delta^{11}B_{borate}$ translates to a 0.5-1.5 unit increase in pH_{cf} relative to ambient pH_{sw} (Cornwall et al., 2017; Donald et al., 2017). Similarly, a wild specimen of *C. nereostratum* exhibited substantially elevated $\delta^{11}B_{cc}$ relative to $\delta^{11}B_{borate}$ of ambient seawater, which was also attributed to the algae's pH_{cf} being at least 0.6 units greater than its ambient pH_{sw} (Fietzke et al., 2015).

The Mg/Ca ratio of calcite has been proposed as a temperature proxy in both inorganically (Berner, 1975) and organically precipitated calcite (Chave, 1954). In coralline algae, the majority of skeletal Mg^{2+} is incorporated into their high-Mg calcite lattice, rather than being associated with organic matter or other Mg-bearing mineral phases (Kamenos et al., 2009; Ries, 2006). The Mg/Ca ratio of coralline algal calcite varies as a function of seawater temperature (e.g. Chave, 1954; Hetzinger et al., 2018; Kamenos et al., 2008; Williams et al., 2014), seawater Mg/Ca (Ries, 2006; Stanley et al., 2002), seawater pH (Ries, 2011), and growth rate (Kolesar, 1978; Moberly, 1968; Sletten et al., 2017) in a manner similar to that of

inorganically precipitated calcite (Gabitov et al., 2014b). The Mg/Ca of coralline algal calcite has also been shown to vary amongst species (through so-called 'vital effects'), and with seasonal cycles in insolation and sea ice cover affecting light levels (Moberly, 1968; Sletten et al., 2017; Adey et al. 2013; Williams et al. 2018). However, these effects are difficult to isolate in wild specimens due to their seasonal covariation. Furthermore, most Mg/Ca-temperature relationships in coralline algae are calibrated using wild specimens grown in poorly constrained seawater temperatures, such as those derived from satellites (Williams et al., 2014), often by averaging temperatures over 2^{o} x 2^{o} latitudinal-longitudinal areas (Hetzinger et al., 2018), and/or by aligning maxima and minima to temporally coordinate the elemental and temperature timeseries (Kamenos et al., 2008). All of these approaches could lead to inaccuracies in the Mg/Ca vs. temperature calibrations and in the final reconstructed seawater temperatures.

Lithium/calcium ratios (Li/Ca) in inorganically precipitated calcite has been shown to vary inversely with temperature (Marriott et al., 2004a; Marriott et al., 2004b). However, the Li/Ca compositions of foraminifera, corals, coralline algae and other marine calcifiers are also influenced by variations in seawater Li/Ca ratio, carbonate ion concentration, calcium carbonate polymorph mineralogy, and calcification rate (Caragnano et al., 2014; Case et al., 2010; Delaney et al., 1985; Dellinger et al., 2018; Fowell et al., 2016; Hall and Chan, 2004; Montagna et al., 2014).

The Mg/Li composition of aragonitic corals (Case et al., 2010; Fowell et al., 2016; Montagna et al., 2014) and calcitic and aragonitic foraminifera (Marchitto et al. 2007; Bryan and Marchitto 2008; Marchitto et al. 2018) exhibits a strong positive dependence on temperature. According to a Rayleigh model of calcification (e.g. Elderfield et al. 1996), growth rate could have similar effects on the partitioning of Li^{+} and Mg^{2+} between the carbonate skeleton and the organism's calcifying fluid. Therefore, dividing Li/Ca by Mg/Ca reduces the secondary impacts of calcification rate on the elemental relationship with temperature, thereby rendering Li/Mg a more reliable recorder of seawater temperature than Li/Ca or Mg/Ca alone (Marchitto et al. 2018; Bryan and Marchitto 2008). However, a prior field-based Mg/Li calibration of the coralline alga *L. kotschyanum* did not show any improvement over the Mg/Ca or Li/Ca temperature proxies (Caragnano et al., 2014).

Here we present the first rigorous calibration of the pH-$\delta^{11}B$ and temperature-Mg/Li relationships for specimens of the arctic/subarctic coralline alga *C. compactum*, which were cultured for 120 days in a controlled laboratory experiment comprising three seawater temperature conditions crossed with four CO_2-manipulated seawater pH conditions.

2.0 Methodology

2.1 Coralline algal cultures

Specimens of *C. compactum* were collected from offshore Acadia National Park, Maine, at a depth of 9-10 m (44° 22' 21.76" N, 68 ° 4' 38.67" W). The coralline algae (Figure 2) were subsequently reared in flow-through seawater aquaria at controlled pCO_2 and temperature conditions. The pCO_2 of the experimental gases were formulated by mixing compressed air and CO_2 with solenoid-valve mass flow controllers, while seawater temperature was controlled with water chillers coupled with 50 W electric heaters. The aquaria were illuminated with 258 µE m^{-2} s^{-1} on a 10:14 hr light:dark cycle. Each experiment was conducted in triplicate 42 L acrylic aquaria, formulated at four pCO_2 levels (1σ): 352 (9), 490 (16), 886 (38), and 3229 (343) µatm and three temperatures (1σ): 6.4 (0.1), 8.8 (0.2), and 12.4 (0.1) ºC, for a total of 12 treatments (Table 1). Seawater from the Gulf of Maine offshore Nahant, Massachusetts, was filtered at 0.2 µm and then pumped through each aquarium at the rate of 75 mL min^{-1}. This flow rate was slow enough to allow the mixed gases to reach near-equilibrium with the experimental seawater, yet fast enough to prevent depletion of dissolved ions within the experimental seawater treatments. The $\delta^{11}B$ composition of each experimental treatment was monitored throughout the duration of the experiment and averaged (1σ) 39.40‰ (0.31), thus within analytical uncertainty of open seawater $\delta^{11}B$ (39.61 ± 0.04 ‰, Foster et al., 2010). The $\delta^{11}B_{borate}$ (average ± uncertainty) of the experimental treatments is derived from equation (1) using measured $\delta^{11}B_{sw}$ and average (+maximum/-minimum) pH_{sw} of each treatment (Table EA1), the latter of which was calculated with the program CO2SYS (Excel, v2.3; Lewis & Wallace 1998) from measurements of total alkalinity and dissolved inorganic carbon, using K_1 and K_2 constants from Roy et al. (1993), the K_{HSO4} constant from Dickson (1990b), and total [B] from Uppstrom (1974).

2.2 Sample preparation and analytical approach

Algal skeleton produced exclusively under experimental conditions was identified relative to a calcein marker emplaced in the skeletons before the start of the experiment. Approximately

3 mg of newly grown skeleton below the tissue layer and meristem, but above the calcein marker, was manually removed with a dental drill. Each sample was then cleaned twice in a clean laboratory fitted with boron-free HEPA filters at the University of Southampton. The cleaning process involved immersing the sample for 15 min in a 500 µL oxidative mixture of 10% hydrogen peroxide buffered with 0.1 M ammonium hydroxide maintained at 80 ^{o}C, and then ultra-sonicating the sample for 5 sec every 5 min, followed by three rinses with Milli-Q water (18.2 MΩ·cm). The samples were leached for 30 seconds with 250 µL 0.0005M nitric acid and then dissolved in a minimal volume of 0.5 M double-distilled nitric acid in 200 µL Milli-Q water in acid-leached *Teflon* vials. Approximately 7% of the sample was then removed for trace element analysis following established techniques (e.g. Donald et al., 2017) on a *Thermo Scientific Element XR* sector-field inductively-coupled-plasma mass spectrometer (ICPMS) at the University of Southampton, with long-term precision (2σ) of in-house consistency standards of 2% (for Mg/Ca) and 4% (for Li/Ca and B/Ca). The remainder of each dissolved sample was processed for δ^{11}B analysis on a *Thermo Scientific Neptune* multicollector ICPMS at the University of Southampton following established protocols (Foster, 2008; Foster et al., 2013). This technique utilized the 10^{12} Omega resistors for the Faraday detectors, resulting in analytical uncertainty of each δ^{11}B measurement (95% confidence, after applying total procedural blank correction) of:

$$2\sigma = 12960e^{-212\left[{}^{11}B\right]} + 0.3385e^{-1.544\left[{}^{11}B\right]}$$

where ^{11}B is voltage on the Faraday detector.

2.3 Statistical analyses

Calibrations were modelled as bivariate least squares linear regressions using the weighted York et al. (2004) approach in Matlab, which accounts for errors in both the X and Y variables (Thirumalai et al., 2011). To account for uncertainties in temperature and $\delta^{11}B_{borate}$, the 95% confidence intervals of the calibration regressions are calculated using a Monte Carlo approach in which 1000 weighted linear regressions are generated by sampling at random within a Gaussian distribution of uncertainty around each variable. Multivariate linear regressions (of the R statistical software; http://www.r-project.org) were used to model covariation between environmental and coralline algal growth parameters, $\delta^{11}B_{cc}$, Mg/Ca, Li/Ca, Mg/Li, and B/Ca composition, Pearson's correlation coefficient (R^2), p-value, t-value, slope, and intercept (where applicable).

3.0 Results

3.1 Boron isotopes of C. compactum

The $\delta^{11}B_{cc}$ of *C. compactum* across all pCO_2 and temperature treatments range from 24.36 ‰ to 30.97 ‰ (Table 1). Specimens grown in different replicate tanks maintained at equivalent pCO_2 and temperature conditions exhibited average variability (1σ) of 0.5 ‰ $\delta^{11}B_{cc}$. The least variability (0.2-0.4 ‰) was observed for the highest temperature treatments and the greatest (up to 1.0 ‰) for the lowest temperature treatments (Table 1). Analyses of $\delta^{11}B_{cc}$ for two specimens within the same replicate tanks of the 9 ºC-470 µatm and 9 ºC-360 µatm treatments revealed within-tank variability in $\delta^{11}B_{cc}$ (grey-shaded cells in Table 1) of 0.07 ‰ and 0.27 ‰, respectively.

3.1.1 The $\delta^{11}B$ – pH proxy

The δ^{11}B-pH proxy is calibrated through the established approach of correlating $\delta^{11}B_{cc}$ with $\delta^{11}B_{borate}$ (instead of correlating $\delta^{11}B_{cc}$ with pH_{sw}) to account for the effects of temperature, salinity, and $\delta^{11}B_{sw}$ composition on $\delta^{11}B_{borate}$. The $\delta^{11}B_{cc}$ of *C. compactum* is consistently greater than seawater $\delta^{11}B_{borate}$ by 12-14 ‰ (Figure 3, Figure EA1), and varies linearly with $\delta^{11}B_{borate}$ pursuant to the regression:

$$\delta^{11}B_{cc}\ (2\sigma) = 1.46\ (0.06)\ \delta^{11}B_{borate} + 6.91\ (0.72)\ (R^2 = 0.9,\ p << 0.01) \qquad (2)$$

Multiple linear regression analysis did not reveal any significant relationships between $\delta^{11}B_{cc}$ and net calcification rate (derived from changes in buoyant weight), seawater temperature, or salinity ($p > 0.05$, Table 2). However, $\delta^{11}B_{cc}$ significantly varied with both linear extension and $\delta^{11}B_{borate}$ ($p << 0.001$, Table 2). Including both linear extension and $\delta^{11}B_{cc}$ in the multivariable regression did not improve the fit of the $\delta^{11}B_{cc}$ vs. $\delta^{11}B_{borate}$ model compared with the weighted bivariate linear regression (Thirumalai et al., 2011) ($R^2 = 0.90$), and instead increased the uncertainty (± 2σ) of the model's slope (± 0.10) and intercept (± 12.31). The $\delta^{11}B_{cc}$ vs. $\delta^{11}B_{borate}$ relationship can be used to reconstruct pH_{sw} by substituting Equation 2 into Equation 1, which yields the following equation:

$$pH_{sw} = pK_B^* - \log\left[-\frac{\delta^{11}B_{sw} - (\delta^{11}B_{cc} - 6.91)/1.46}{\delta^{11}B_{sw} - (\alpha_B(\delta^{11}B_{cc} - 6.91)/1.46 - 1000\left(\alpha_B - 1\right))}\right] \qquad (3)$$

The uncertainty of the $\delta^{11}B_{cc}$ vs. $\delta^{11}B_{borate}$ regression is illustrated with the 95% confidence interval (dashed envelope in Figure 3) and contributes an average error of 0.03 to reconstructed pH, which increases towards lower seawater pH. The total uncertainty of reconstructed pH includes also the uncertainty of the $\delta^{11}B_{cc}$ analyses, and is therefore sample-specific. For the algal specimens used to develop the calibration, reconstructed pH exhibits an average uncertainty of +0.05/-0.10 pH units, with 31 of the 36 reconstructed pH values (including associated uncertainty) overlapping the corresponding measured seawater pH range, indicating that reconstructed pH faithfully represents seawater pH (Figure EA2).

3.1.2 Calcifying fluid pH from $\delta^{11}B_{cc}$

Assuming that boron in the skeleton of *C. compactum* is derived solely from borate ion in the alga's calcifying fluid, $\delta^{11}B_{cc}$ can also be used to calculate pH_{cf} (Table 1) and its relative offset from pH_{sw} (ΔpH), expressed here also as the difference in the concentration of protons between seawater and calcifying fluid ($\Delta[H^+]$). As expected from the $\delta^{11}B_{cc}$ vs. $\delta^{11}B_{borate}$ relationship, pH_{cf} is strongly positively correlated with pH_{sw} ($R^2 = 0.8$, $p << 0.01$, Figure 4a). Notably, ΔpH increases from ~1 to 1.6 and $\Delta[H^+]$ decreases from $-0.6*10^{-8}$ to $-6.5*10^{-8}$ M with a decrease in pH_{sw} from 8.1 to 7.2 (Figure 4b), suggesting that the algae are removing more protons from their calcifying fluid under more acidic seawater conditions.

3.2 *B/Ca in* C. compactum

Boron/calcium ratios (B/Ca) in the investigated *C. compactum* specimens range from 320 to 430 μmol/mol amongst treatments (Table 1), a smaller range of B/Ca compared to that within the skeleton of the branching coralline alga *Neogoniolithon* sp. (350 to 750 μmol/mol) when cultured over a similar range of pH_{sw} (Donald et al., 2017). The lower sensitivity of B/Ca to pCO_2 and temperature of the experimental treatments within *C. compactum* compared to *Neogoniolithon* sp., and the large average standard deviation in B/Ca (27 μmol/mol) amongst treatment replicates, hinder development of robust regressions between B/Ca and pH_{sw} or temperature. Here because of the consistently higher B/Ca at higher $\delta^{11}B_{cc}$ within the coralline algae, (Figure EA3) is used solely as evidence towards the assertion that dissolved borate ion is the primary form of B incorporated into the coralline algal calcite. For consistency with the analyses of skeletal Mg/Ca and Li/Ca, multivariate regression analysis is used to evaluate the relationship between B/Ca and temperature, pH_{sw}, growth rate, and linear extension (Table 2).

3.3 Mg/Li-temperature relationships in C. compactum

Coralline algal Mg/Ca ratios range from 115 to 170 mmol/mol, consistent with other studies on *Clathromorphum* sp. (Williams et al., 2014), with replicate samples yielding average standard deviation of 8 mmol/mol (Table 1). Multivariate regression analysis (Table 2) reveals that neither temperature nor pH_{sw} have a statistically significant relationship with skeletal Mg/Ca ($p>0.5$), although Mg/Ca was found to significantly vary with linear extension rate ($p<0.01$) (Table 2, Figure EA4). The Li/Ca composition of *C. compactum* ranges from 40 to 77 μmol/mol, more than four times the Li/Ca composition of the coralline alga *Lithophyllum kotschyanum* (Caragnano et al., 2014), with replicate samples yielding average standard deviation of 5 μmol/mol. A similar multivariate regression analysis of Li/Ca within *C. compactum* specimens reveals a strong, statistically significant inverse relationship with temperature ($p<0.01$) and a weaker but still statistically significant relationship with linear extension ($p<0.05$) (Table 2, Figure EA4). Similar to Mg/Ca, Li/Ca does not significantly vary with pH_{sw} ($p=0.1$). Mg/Ca is highly variable across the skeleton in *Clathromorphum*, a phenomenon previously attributed to different modes and/or rates of calcification across the skeleton (Fietzke et al. 2015), potentially owing to differences in light intensity (Williams et al., 2018). We suspect that Li/Ca ratios in *C. compactum* are linked to similar processes based upon the significant correlation between skeletal extension rate and skeletal Li/Ca.

Notably, skeletal Mg/Li was found to exhibit a stronger relationship with temperature (R^2 = 0.7, $p<<0.01$, Figure 5) than either Mg/Ca or Li/Ca alone, yielding the following equation:

$$Mg/Li\ (2\sigma) = 0.17\ (0.02) * temperature\ (^{o}C) + 1.02\ (0.16)$$

Based on the 95% confidence interval of the regression (considering error on both temperature and Mg/Li), coralline algal Mg/Li ratios yield seawater temperatures with an uncertainty of 0.5 ^{o}C within the temperature range of 7.5 - 11.5^{o}C, up to an uncertainty of 1.5 ^{o}C at the extreme ends of the regression. Although there is relatively high variability in Mg/Li amongst replicate specimens, averaging 2-3 replicate specimens brings Mg/Li values (solid grey circles, Figure 5) within the 95% confidence interval of the calibration regression.

4.0 Discussion

4.1 Boron isotope – pH proxy in C. compactum

Boron isotopes have been employed in a variety of calcium carbonate precipitating marine organisms to reconstruct pH_{sw} (Foster, 2008; Hönisch et al., 2009; Pelejero et al., 2005; Wei et al., 2009). Even in coralline algae, where calcification can occur extracellularly but within fluids bounded by adjacent algal cell walls, skeletal boron isotopes reflect pH_{sw} with varying degrees of species-specific biological control (Cornwall et al., 2017; Donald et al., 2017). Assuming that borate is the primary form of boron incorporated into the skeleton of *C. compactum*, the elevated $\delta^{11}B$ of the coralline algal skeleton relative to that expected from the $\delta^{11}B_{borate}$-pH_{sw} relationship suggests that pH within the alga's zone of calcification is higher than pH of the surrounding seawater (shown as pH_{cf} vs. pH_{sw} in Figure 4a and ΔpH and $\Delta[H^+]$ in Figure 4b). This could promote calcification in a manner similar to foraminifera (De Nooijer et al., 2014), corals (Al-Horani et al., 2003; Holcomb et al., 2014; Krief et al., 2010; McCulloch et al., 2012; Venn et al., 2011), and other species of marine calcifiers (Sutton et al., 2018).

As with *Neogoniolithon* sp. (Donald et al., 2017) and some cold water corals (Stewart et al., 2016), *C. compactum* $\delta^{11}B_{cc}$ is positively correlated with $\delta^{11}B_{borate}$ and skeletal B/Ca (Figures 3, 5). However, the $\delta^{11}B_{cc}$ - pH_{sw} relationship of *C. compactum* is more linear than that observed for the tropical, branching coralline algae *Neogoniolithon* sp. (Donald et al., 2017). This underscores the importance of developing species-specific calibrations for the algal $\delta^{11}B_{cc}$ - pH_{sw} proxy. Importantly, B/Ca and $\delta^{11}B_{cc}$ are both highly positively correlated with pH_{sw} (Table 2), which is qualitatively consistent with the assumption that dissolved borate ion is the primary form of B incorporated into coralline algal calcite (Cornwall et al., 2017; Donald et al., 2017; Zeebe and Wolf-Gladrow, 2001). As with previous studies (Donald et al., 2017), there is a parabolic relationship between pH_{sw} and calcification rate (derived from change in buoyant weight) and linear extension (Table 1, Figure EA5). If lower calcification rates are accompanied by increased incorporation of boric acid in the coralline alga skeleton, as observed in experiments on inorganically precipitated calcite (Noireaux et al., 2015; Farmer et al. 2019), this would weaken the linear relationship between $\delta^{11}B_{cc}$ and $\delta^{11}B_{borate}$ by increasing the offset between $\delta^{11}B_{cc}$ and $\delta^{11}B_{borate}$ (and inflate the calculated ΔpH) for both low and high seawater pH treatments. That this phenomenon was not observed in the present study (Figure 4b) suggests that if present, any boric acid incorporation into the algal skeleton does not systematically vary with algal calcification rate and pH.

403 The slopes and intercepts of the relationship between $\delta^{11}B_{cc}$ and seawater $\delta^{11}B_{borate}$ are greater
404 in *C. compactum* than in most other marine carbonates (slope of 1.5 vs. ≤ 1, y-intercept of 6.9
405 vs. ≤ 3, (Foster and Rae, 2016; Stewart et al., 2016 and references therein)), and the
406 sensitivity (slope) and offset (intercept) of *C. compactum* pH_{cc} to seawater pH_{sw} is larger than
407 in other species of coralline algae studied to date (Figure 4a). The apparent increase in $\delta^{11}B_{cc}$
408 (pH_{cf}) relative to $\delta^{11}B_{borate}$ (pH_{sw}), and the increase in absolute magnitude of both ΔpH and
409 $\Delta[H^+]$ with decreasing pH_{sw} collectively suggest that *C. compactum* allocates substantial
410 energy to maintaining conditions favourable for calcification (i.e., expelling H^+, increasing
411 pH at the site of calcification). This may contribute to this species' ability to occupy a wide
412 geographic and, thus, environmental range, despite its highly soluble high-Mg calcite
413 skeleton, including in Arctic and subarctic waters where they experience lower pH and
414 calcium carbonate saturation states than in warmer waters.
415
416 The $\delta^{11}B_{cc}$ of *C. compactum* exhibited a weak but statistically significant relationship with
417 linear extension rate even after accounting for the confounding effects of carbonate chemistry
418 on algal growth and $\delta^{11}B_{cc}$ (Table 2). This is important from a physiological perspective
419 because it suggests that growth of *C. compactum* is enhanced by elevating pH at the site of
420 calcification. The relationship between growth and $\delta^{11}B_{cc}$ was not evident for the tropical
421 coralline alga *Neogoniolithon* sp. (Donald et al., 2017), indicating that it is not consistent
422 across all species of coralline algae. However, net calcification rate (i.e., gross calcification
423 minus gross dissolution) within *C. compactum*, estimated from changes in buoyant weight of
424 the coralline algae, did not vary significantly with $\delta^{11}B_{cc}$ (Table 2). On the contrary, $\delta^{11}B_{cc}$
425 and net calcification rate within *Neogoniolithon* sp. covaried in the pH range of 7.64 - 8.08
426 (Cornwall et al., 2017), providing additional evidence of interspecific differences in algal
427 growth-$\delta^{11}B_{cc}$ relationships. The discrepancy between trends in linear extension vs. $\delta^{11}B_{cc}$
428 and net calcification vs. $\delta^{11}B_{cc}$ may arise from the dissolution of exposed skeleton in the
429 undersaturated treatments having a more negative impact on net calcification than on linear
430 extension. Furthermore, this species of coralline algae are able to calcify even during
431 prolonged periods of darkness, both in aquaria and in the wild during the dark months of the
432 Arctic/subarctic winter (Adey et al., 2013). This suggests that the observed elevation of pH_{cf}
433 relative to pH_{sw} (estimated from elevation of $\delta^{11}B_{cc}$ relative to $\delta^{11}B_{borate}$) is not solely driven
434 by light-induced photosynthetic drawdown of inorganic carbon, but could be instead driven
435 by active removal of protons from the alga's calcifying fluid. This, in concert with the

deployment of chitin, collagen, and proteinaceous polysaccharides (Rahman and Halfar, 2014), may promote the formation and stabilization of coralline algal skeleton independent of light availability, which would confer a high degree of plasticity to this alga's mechanism of calcification.

The ability of *C. compactum* to modify its pH_{cf} might also be the reason for the small degree of variance in its $\delta^{11}B$ amongst within-treatment replicates (Table 1), compared with other species of coralline algae, such as *Neogoniolithon* sp. (Donald et al., 2017), that have been investigated in similarly designed experiments. Nevertheless, the standard deviation in $\delta^{11}B_{cc}$ amongst within-treatment replicates of *C. compactum* exhibits a statistically significant ($p = 0.03$) inverse relationship with water temperature (from 6 to 12 ºC), but no significant relationship with pH_{sw} ($p = 0.8$), suggesting that *C. compactum* has less control over pH_{cf} at lower temperatures. This is consistent with prior field-based observations (Adey et al., 2013) that the optimal temperature range for growth of this species is 11-12 ^{o}C. Therefore, assuming that coralline algae have more energy available for controlling pH_{cf} when inhabiting waters closer to their thermal optimum, these results support the assertion that controlling pH_{cf} is energetically expensive (McCulloch et al., 2012).

4.2 Mg/Li – temperature proxy

Multivariate linear regression analysis revealed that the skeletal Mg/Ca ratio of *C. compactum* varied significantly with rates of linear extension, but not with seawater temperature (Table 1). These results suggest that field-based Mg/Ca-temperature calibrations of *Clathromorphum* (Gamboa et al., 2010; Hetzinger et al., 2010; Williams et al., 2014) could at least partly reflect temperature-induced changes in calcification rate on skeletal Mg/Ca ratios (Gabitov et al., 2014a; Kolesar, 1978; Moberly, 1968; Sletten et al., 2017). Alternatively, the strong seasonal relationships between seawater temperature and algal skeletal Mg/Ca observed in the field may arise from seasonal variations in light intensity and/or ice cover (Halfar et al., 2013; Williams et al. 2018) that are correlated with temperature. Those relationships may also simply be more evident in the field than in the present laboratory experiment where the seasonal range of temperatures is larger than the 6 - 12 ºC range employed in the experiment.

The Li/Ca ratios in *C. compactum* exhibited a strong inverse relationship with seawater temperature, and a relatively small but statistically significant relationship with linear

extension rate (Table 2). This constitutes a novel proxy for seawater temperature within coralline algae. Since the effect of extension rate on Mg/Ca and Li/Ca is in the same direction, dividing skeletal Mg/Ca by Li/Ca to yield Mg/Li ratios effectively reduces the confounding effects of linear extension on the Mg/Li-temperature proxy (Figure 5; Table 2).

The sensitivity of the Mg/Li ratio to seawater temperature is approximately 10-fold greater for *C. compactum* than for aragonitic carbonates (Marchitto et al. 2018; Montagna et al., 2014; Fowell et al. 2016) and calcitic foraminifera (Marchitto et al. 2007; Bryan and Marchitto 2008) (Figure 5). This is potentially driven by differences in mineralogy, with *C. compactum* containing approximately 30-fold higher Mg/Ca and 3-fold higher Li/Ca ratio relative to coral and foraminiferal aragonite and foraminiferal calcite, and calcification mechanisms amongst these organisms.

Although mechanisms of calcification within coralline algae remain poorly understood and likely vary amongst species, there is evidence that calcification occurs within semi-isolated regions and could therefore exhibit evolution of elemental chemistry as a function of calcification rate, modified by rate of seawater exchange, ion transport, and other factors, such as elemental binding via organic templates and ion entrapment (Marchitto et al. 2018; Gabitov et al., 2014a; Gabitov et al., 2011; Gagnon et al., 2012). All of these processes have the potential to influence elemental partitioning within different structural components of coralline algal calcite under different growth rate and temperature regimes. Nevertheless, the strong correlation between *C. compactum* Mg/Li and seawater temperature, in a manner similar to that observed within aragonitic corals and foraminifera, and provides the first compelling empirical support for the viability of this temperature proxy within *C. compactum*.

5.0 Conclusions

Strong and statistically significant relationships were identified between skeletal $\delta^{11}B_{cc}$ and seawater $\delta^{11}B_{borate}$ (which varies as a function of pH_{sw}), and between skeletal Mg/Li and seawater temperature, for specimens of the encrusting coralline alga *C. compactum* cultured for approximately 120 days in a controlled pCO_2-temperature experiment. These relationships permitted development of a $\delta^{11}B$-based proxy of seawater pH and a Mg/Li-based proxy of seawater temperature for *C. compactum*, with regression specific average uncertainties of 0.03 pH units and 0.7-1.5 ^{o}C, respectively. The observed elevation of $\delta^{11}B_{cc}$

relative to $\delta^{11}B_{borate}$ suggests that this species of coralline red alga calcifies from a semi-isolated fluid of substantially elevated pH (1.0-1.6 pH units) relative to that of its ambient seawater, with the degree of proton (and thus pH) modification increasing with decreasing seawater pH. The relatively low variance in $\delta^{11}B_{cc}$ amongst replicate specimens within treatments provides further empirical support for the viability of the *C. compactum* δ^{11}B-pH proxy. The combined Li/Ca-Mg/Ca (i.e., Mg/Li) proxy was more significantly related to temperature than Li/Ca alone, apparently due to reduction of the confounding effects of skeletal extension rate on Li/Ca and Mg/Ca elemental partitioning in the skeleton achieved by dividing the two ratios. This species of coralline red alga may be particularly useful in paleoceanographic reconstructions because of its annually layered skeletons and its widespread distribution in the Arctic and subarctic oceans. Their growth can span a millennium, potentially providing long-term, annually resolved records of ocean acidification and warming in ocean basins historically lacking in these proxy records.

Acknowledgements

JBR and BW acknowledge funding from NSF MGG grants #1459706 and 1459827. We thank Cait Cleaver and Phoebe Jekielek for collecting the algal specimens, and the Schoodic Institute at Acadia National Park for supporting the fieldwork. We also thank Andy Milton for assistance with analytical instrumentation.

Formatting of funding sources

NSF MGG grants #1459706 and # 1459827

Figure captions

Figure 1: Geographic distribution of *Clathromorphum* species in the Arctic and subarctic oceans (Adey et al., 2013). Distribution of *C. nereostratum* is shown in yellow and *C. compactum* in red on a map from Google Earth (Image: Landsat/Copernicus, IBCAO, USGS, Data: SIO, NOAA, U.S. Navy, NGA, GEBCO). Star indicates the sampling location of the species used in this study.

Figure 2: Cross section through a *Clathromophum* skeleton showing the meristem, perithallium, and epithallium structures (Williams et al., 2018).

Figure 3: Weighted linear regression between skeletal $\delta^{11}B$ ($\delta^{11}B_{cc}$) of *C. compactum* and $\delta^{11}B$ of seawater borate ($\delta^{11}B_{borate}$). The uncertainties on both axes were accounted for in generating both the regression and its 95% confidence interval (see Methods for details).

Figure 4: Relationships between seawater pH (pH_{sw}), pH recorded by the coralline algae (pH_{cf}), and proton differentials between the two. (a) Linear regression of pH_{cf} vs. pH_{sw} for *C. compactum* in the present study. Previously published relationships of pH_{cf} vs. pH_{sw} for three other species of coralline algae are shown for comparison. The solid line shows the 1:1 relationship between pH_{cf} and pH_{sw}. (b) pH offset ($\Delta pH = pH_{cf} - pH_{sw}$) and proton concentration difference ($\Delta[H^+] = [H^+]_{cf} - [H^+]_{sw}$) between the calcifying fluid and ambient seawater of *C. compactum*, as a function of pH_{sw}. Red circles denote $\Delta[H^+]$ and blue circles represent ΔpH.

Figure 5: Relationship between skeletal Mg/Li and seawater temperature. Weighted linear regression of skeletal Mg/Li vs. seawater temperature is shown with solid blue line and 95% confidence interval of the regression is shown with dotted light blue curves (see Methods). The solid grey circles represent replicate means. For comparison, Mg/Li-temperature relationships are shown for aragonitic corals (dashed double dot line: Montagna et al., 2014; dotted line: Fowell et al., 2016), for the aragonitic foraminifera *H. elegans* (dash-dot line), and for calcitic foraminifera (black dashed line: *C. pachyderma*; blue dashed line: *P. ariminensis*; red dashed line: *P. foveolata*; purple dashed line: *U. peregrina*) (Bryan and Marchitto 2008; Marchitto et al. 2007). Error bars on temperature represent variability (1σ) throughout the duration of the experiment (Table EA1); error bars on Mg/Li represent long-term precision (2σ) of in-house consistency standards as described in Methods.

Additional material:

Table 1, Table 2, Electronic supplement (Figure EA1, Figure EA2, Figure EA3, Figure EA4, Figure EA5, Table EA1)

References

Adey, W.H. (1979) Crustose coralline algae as microenvironmental indicators for the Tertiary, in: Boucot, A., Gray, J. (Eds.), Historical Biogeography, Plate Tectonics and the Changing Environment, pp.500.

571 Adey, W.H. (1998) Coral Reefs: algal structured and mediated ecosystems in shallow,
572 turbulent alkaline waters. J. Phycol. 34, 393-406.
573 Adey, W.H., Halfar, J.a. and Williams, B. (2013) The coralline genus *Clathromorphum*
574 *Foslie* emend. Adey: Biological, physiological, and ecological factors controlling carbonate
575 production in an Arctic-Subarctic climate archive. Smithson. Contrib. Mar. Sci. 40, 1-41.
576 Adey, W.H., Lindstrom, S.C., Hommersand, M.H. and Müller, K.M. (2008) The
577 biogeographic origin of Arctic endemic seaweeds: a thermographic view. J. Phycol. 44,
578 1384-1394.
579 Al-Horani, F.A., Al-Moghrabi, S.M. and de Beer, D. (2003) The mechanism of calcification
580 and its relation to photosynthesis and respiration in the scleractinian coral Galaxea
581 fascicularis. Mar. Biol. 142, 419-426.
582 Alexandersson, E.T. (1974) Carbonate cementation in coralline algal nodules in the
583 Skagerrak, North Sea: biochemical precipitation in undersaturated waters. J. Sed. Petrol. 44,
584 7–26.
585 Anagnostou, E., Huang, K.F., You, C.F., Sikes, E.L. and Sherrell, R.M. (2012) Evaluation of
586 boron isotope ratio as a pH proxy in the deep sea coral *Desmophyllum dianthus*: Evidence of
587 physiological pH adjustment. Earth Plan. Sci. Lett. 349, 251-260.
588 Beer, D.D. and Larkum, A.W.D. (2001) Photosynthesis and calcification in the calcifying
589 algae Halimeda discoidea studied with microsensors. Plant Cell Environ. 24, 1209-1217.
590 Berner, R.A. (1975) The role of magnesium in the crystal growth of calcite and aragonite
591 from sea water. Geochim. Cosmochim. Acta 39, 489-504.
592 Borowitzka, M.A. and Larkum, A.W.D. (1987) Calcification in algae: Mechanisms and the
593 role of metabolism. Crit Rev Plant Sci 6, 1-45.
594 Bryan, S.P., and Marchitto, T.M. (2008) Mg/Ca-temperature proxy in benthic foraminifera:
595 new calibrations from the Florida Straits and a hypothesis regarding Mg/Li.
596 Paleoceanography 23, PA2220.
597 Burdett, H., Kamenos, N.A. and Law, A. (2011) Using coralline algae to understand historic
598 marine cloud cover. Palaeogeo Palaeoclim Palaeoecol 302, 65-70.
599 Caragnano, A., Basso, D., Jacob, D.E., Storz, D., Rodondi, G., Benzoni, F. and Dutrieux, E.
600 (2014) The coralline red alga *Lithophyllum kotschyanum* f. affine as proxy of climate
601 variability in the Yemen coast, Gulf of Aden (NW Indian Ocean). Geochim. Cosmochim.
602 Acta 124, 1-17.
603 Case, D.H., Robinson, L.F., Auro, M.E. and Gagnon, A.C. (2010) Environmental and
604 biological controls on Mg and Li in deep-sea scleractinian corals. Earth Plan. Sci. Lett. 300,
605 215-225.
606 P. Chan, P., Halfar, J., Norley, C. J. D., Pollmann, S. I., Adey, W., Holdsworth, D. W. (2017)
607 Micro-computed tomography: Applications for high-resolution skeletal density
608 determinations: An example using annually banded crustose coralline algae. Geochem.
609 Geophys. Geosys. 18, 3542-3553.
610 Chan, P., Halfar, J., Williams, B., Hetzinger, S., Steneck, R., Zack, T. and Jacob, D.E. (2011)
611 Freshening of the Alaska Coastal Current recorded by coralline algal Ba/Ca ratios. J.
612 Geophys. Res. 116, G01032.
613 Chave, K.E. (1954) Aspects of the biogeochemistry of magnesium 1. Calcareous marine
614 organisms. J. Geology 62, 266-283.
615 Chenelot, H., Jewett, S.C. and Hoberg, M.K. (2011) Macrobenthos of the nearshore Aleutian
616 Archipelago, with emphasis on invertebrates associated with *Clathromorphum nereostratum*
617 (Rhodophyta, Corallinaceae). Mar. Biodiversity 41, 413-424.
618 Comeau, S., Carpenter, R.C. and Edmunds, P.J. (2013) Coral reef calcifiers buffer their
619 response to ocean acidification using both bicarbonate and carbonate. Proc Royal Soc B: Biol
620 Sci 280, 20122374.

Cornwall, C.E., Comeau, S. and McCulloch, M.T. (2017) Coralline algae elevate pH at the site of calcification under ocean acidification. Glob Change Biol 23, 4245-4256.
De Nooijer, L. J., S., H. J., E., J., B., J., and Reichart, G.J. (2014) Biomineralization in perforate foraminifera. Earth Plan. Sci. Lett. 135, 48-58.
Delaney, M.L., W.H.Bé, A. and Boyle, E.A. (1985) Li, Sr, Mg, and Na in foraminiferal calcite shells from laboratory culture, sediment traps, and sediment cores. Geochim. Cosmochim. Acta 49, 1327-1341.
Dellinger, M., West, A.J., Paris, G., Adkins, J.F., Pogge von Strandmann, P.A.E., Ullmann, C.V., Eagle, R.A., Freitas, P., Bagard, M.-L., Ries, J.B., Corsetti, F.A., Perez-Huerta, A. and Kampf, A.R. (2018) The Li isotope composition of marine biogenic carbonates: Patterns and mechanisms. Geochim. Cosmochim. Acta.
Dickson, A.G. (1990a) Thermodynamics of the dissociation of boric acid in synthetic seawater from 273.15 to 318.15 K. Deep-Sea Res. 37, 755-766.
Dickson, A.G. (1990b) Standard potential of the reaction: $AgCl(s) + 12H_2(g) = Ag(s) + HCl(aq)$, and and the standard acidity constant of the ion HSO_4^- in synthetic sea water from 273.15 to 318.15 K. J. Chem. Thermodynam. 22,113-127.
Digby, P.S.B. (1977) Photosynthesis and respiration in the coralline algae, *Clathromorphum circumscriptum* and *Corallina officinalis* and the metabolic basis of calcification. J. Mar. Biol. Assoc. United Kingdom 57, 1111-1124.
Donald, H.K., Ries, J.B., Stewart, J.A., Fowell, S.E. and Foster, G.L. (2017) Boron isotope sensitivity to seawater pH change in a species of Neogoniolithon coralline red alga. Geochim. Cosmochim. Acta 217, 240-253.
Elderfield, H., Bertram, C.J., and Erez, J. (1996) A biomineralization model for the incorporation of trace elements into foraminfieral calcium carbonate. Earth Plan. Sci. Lett. 142, 409-423.
Fabricius, K.E., Kluibenschedl, A., Harrington, L., Noonan, S. and De'ath, G. (2015) In situ changes of tropical crustose coralline algae along carbon dioxide gradients. Sci. Rep. 5, 9537.
Farmer, J.R, Branson, O., Uchikawa, J., Penman, D.E., Hönisch, B., Zeebe, R.E. (2019) Boric acid and borate incorporation in inorganic calcite inferred from B/Ca, boron isotopes and surface kinetic modeling, Geochim. Cosmochim. Acta 244, 229-247.
Fietzke, J., Ragazzola, F., Halfar, J., Dietze, H., Foster, L.C., Hansteen, T.H., Eisenhauer, A. and Steneck, R.S. (2015) Century-scale trends and seasonality in pH and temperature for shallow zones of the Bering Sea. Proc Nat Ac Sci 112, 2960-2965.
Foster, G.L. (2008) Seawater pH, pCO_2 and $[CO_3^{2-}]$ variations in the Caribbean Sea over the last 130 kyr: A boron isotope and B/Ca study of planktic foraminifera. Earth Plan. Sci. Lett. 271, 254-266.
Foster, G.L., Hönisch, B., Paris, G., Dwyer, G.S., Rae, J.W.B., Elliott, T., Gaillardet, J., Hemming, N.G., Louvat, P. and Vengosh, A. (2013) Interlaboratory comparison of boron isotope analyses of boric acid, seawater and marine $CaCO_3$ by MC-ICPMS and NTIMS. Chem. Geol. 358, 1-14.
Foster, G.L., Pogge von Strandmann, P.A.E. and Rae, J.W.B. (2010) Boron and magnesium isotopic composition of seawater. Geochem. Geophys. Geosyst. 11, Q08015.
Foster, G.L. and Rae, J.W.B. (2016) Reconstructing ocean pH with boron isotopes in foraminifera. Ann Rev Earth Plan Sci 44, 207-237.
Fowell, S.E., Sandford, K., Stewart, J.A., Castillo, K.D., Ries, J.B. and Foster, G.L. (2016) Intrareef variations in Li/Mg and Sr/Ca sea surface temperature proxies in the Caribbean reef-building coral *Siderastrea siderea*. Paleoceanography 31, 1315-1329.
Frantz, B.R., Foster, M.S. and Riosmena-Rodríguez, R. (2005) *Clathromorphym nereostratum* (Corallinales, Rhodophyta): The oldest alga? J. Phycol. 41, 770-773.

Gabitov, R.I., Rollion-Bard, C., Tripati, A. and Sadekov, A. (2014a) In situ study of boron partitioning between calcite and fluid at different crystal growth rates. Geochim. Cosmochim. Acta 137, 81-92.
Gabitov, R.I., Sadekov, A. and Leinweber, A. (2014b) Crystal growth rate effect on Mg/Ca and Sr/Ca partitioning between calcite and fluid: An in situ approach. Chem. Geol. 367, 70-82.
Gabitov, R.I., Schmitt , A.K., Rosner, M., McKeegan, K.D., Gaetani, G.A., Cohen, A.L., Watson, E.B. and Harrison, T.M. (2011) In situ δ^7Li, Li/Ca, and Mg/Ca analyses of synthetic aragonites. Geochem. Geophys. Geosys. 12.
Gaetani, G.A., Cohen, A.L., Wang, Z. and Crusius, J. (2011) Rayleigh-based, multi-element coral thermometry: A biomineralization approach to developing climate proxies. Geochim. Cosmochim. Acta 75, 1920-1932.
Gagnon, A.C., Adkins, J.F. and Erez, J. (2012) Seawater transport during coral biomineralization. Earth Plan. Sci. Lett. 329-330, 150-161.
Gagnon, A.C., Adkins, J.F., Fernandez, D.P. and Robinson, L.F. (2007) Sr/Ca and Mg/Ca vital effects correlated with skeletal architecture in a scleractinian deep-sea coral and the role of Rayleigh fractionation. Earth Plan. Sci. Lett. 261, 280-295.
Gamboa, G., Halfar, J., Hetzinger, S., Adey, W., Zack, T., Kunz, B. and Jacob, D.E. (2010) Mg/Ca ratios in coralline algae record northwest Atlantic temperature variations and North Atlantic Oscillation relationships. J. Geophys. Res: Oceans 115, C12044.
Gao, K., Aruga, Y., Asada, K., Ishihara, T., Akano, T. and Kiyohara, M. (1993) Calcification in the articulated coralline alga *Corallina pilulifera*, with special reference to the effect of elevated CO2 concentration. Mar. Biol. 117, 129-132.
Halfar, J., Adey, W.H., Kronz, A., Hetzinger, S., Edinger, E. and Fitzhugh, W.W. (2013) Arctic sea-ice decline archived by multicentury annual-resolution record from crustose coralline algal proxy. Proc. Nat. Acad. Sci. 110, 19737-19741.
Halfar, J., Hetzinger, S., Adey, W., Zack, T., Gamboa, G., Kunz, B., Williams, B. and Jacob, D.E. (2011) Coralline algal growth-increment widths archive North Atlantic climate variability. Palaeogeo. Palaeoclim. Palaeoecol. 302, 71-80.
Halfar, J., Steneck, R., Schöne, B., Moore, G.W.K., Joachimski, M., Kronz, A., Fietzke, J. and Estes, J. (2007) Coralline alga reveals first marine record of subarctic North Pacific climate change. Geophys. Res. Lett. 34, L07702.
Hall, J.M. and Chan, L.H. (2004) Li/Ca in multiple species of benthic and planktonic foraminifera: thermocline, latitudinal, and glacial-interglacial variation Geochim. Cosmochim. Acta 68, 529-545.
Hemming, N.G. and Hanson, G.N. (1992) Boron isotopic composition and concentration in modern marine carbonates. Geochim. Cosmochim. Acta 56, 537-543.
Hetzinger, S., Halfar, J., Kronz, A., Simon, K., Adey, W.H. and Steneck, R.S. (2018) Reproducibility of *Clathromorphum compactum* coralline algal Mg/Ca ratios and comparison to high-resolution sea surface temperature data. Geochim. Cosmochim. Acta 220, 96-109.
Hetzinger, S., Halfar, J., Kronz, A., Steneck, R.S., Adey, W., Lebednik, P. and Schöne, B.R. (2009) High-resolution Mg/Ca ratios in a coralline red alga as a proxy for Bering Sea tenperature variations from 1902 to 1967. PALAIOS 24, 406-412.
Hetzinger, S., Pfeiffer, M., Dullo, W.-C., Garbe-Schönberg, D. and Halfar, J. (2010) Rapid 20th century warming in the Caribbean and impact of remote forcing on climate in the northern tropical Atlantic as recorded in a Guadeloupe coral. Palaeogeo Palaeoclim Palaeoecol 296, 111-124.
Heyward, A.J. and Negri, A.P. (1999) Natural inducers for coral larval metamorphosis. Coral Reefs 18, 273-279.

719 Hoegh-Guldberg, O., Mumby, P.J., Hooten, A.J., Steneck, R.S., Greenfield, P., Gomez, E.,
720 Harvell, C.D., Sale, P.F., Edwards, A.J., Caldeira, K., Knowlton, N., Eakin, C.M., Iglesias-
721 Prieto, R., Muthiga, N., Bradbury, R.H., Dubi, A. and Hatziolos, M.E. (2007) Coral Reefs
722 Under Rapid Climate Change and Ocean Acidification. Science 318, 1737-1742.
723 Hofmann, L.C., Koch, M. and de Beer, D. (2016) Biotic Control of Surface pH and Evidence
724 of Light-Induced H+ Pumping and Ca2+-H+ Exchange in a Tropical Crustose Coralline
725 Alga. PLoS One 11, e0159057.
726 Holcomb, M., Venn, A.A., Tambutté, E., Tambutté, S., Allemand, D., Trotter, J. and
727 McCulloch, M. (2014) Coral calcifying fluid pH dictates response to ocean acidification. Sci.
728 Rep. 4, 5207.
729 Hönisch, B., Hemming, N.G., Archer, D., Siddall, M. and McManus, J.F. (2009)
730 Atmospheric carbon dioxide concentration across the Mid-Pleistocene transition. Science
731 324, 1551-1554.
732 Hurd, C.L., Cornwall, C.E., Currie, K., Hepburn, C.D., McGraw, C.M., Hunter, K.A. and
733 Boyd, P.W. (2011) Metabolically induced pH fluctuations by some coastal calcifiers exceed
734 projected 22nd century ocean acidification: a mechanism for differential susceptibility? Glob
735 Change Biol 17, 3254-3262.
736 Kamenos, N.A. (2012) Reconstructing Greenland ice sheet runoff using coralline algae.
737 Geology 40, 1095-1098.
738 Kamenos, N.A., Cusack, M., Huthwelker, T., Lagarde, P. and Scheibling, R.E. (2009) Mg-
739 lattice associations in red coralline algae. Geochim. Cosmochim. Acta 73, 1901-1907.
740 Kamenos, N.A., Cusack, M. and Moore, P.G. (2008) Coralline algae are global
741 palaeothermometers with bi-weekly resolution. Geochim. Cosmochim. Acta 72, 771-779.
742 Kamenos, N.A. and Law, A. (2010) Temperature controls on coralline algal skeletal growth.
743 J. Phycol. 46, 331-335.
744 Klochko, K., Kaufman, A.J., Yoa, W., Byrne, R.H. and Tossell, J.A. (2006) Experimental
745 measurement of boron isotope fractionation in seawater. Earth Plan. Sci. Lett. 248, 261-270.
746 Kolesar, P.T. (1978) Magnesium in calcite from a coralline alga. J. Sed. Petrol. 48, 815-819.
747 Krief, S., Hendy, E.J., Fine, M., Yam, R., Meibom, A., Foster, G.L. and Shemesh, A. (2010)
748 Physiological and isotopic responses of scleractinian corals to ocean acidification. Geochim.
749 Cosmochim. Acta 74, 4988-5001.
750 Lewis, E. and Wallace, D. W. R. (1998) Program developed for CO_2 system calculations,
751 ORNL/CDIAC-105, Carbon Dioxide Inf. Anal. Cent., Oak Ridge Natl. Lab., Oak Ridge,
752 Tenn., 38 pp.
753 Liu, W., Xie, S.-P., Liu, Z. and Zhu, J. (2017) Overlooked possibility of a collapsed Atlantic
754 Meridional Overturning Circulation in warming climate. Science Advances 3.
755 Marchitto, T.M., Bryan, S.P., Doss, W., McCulloch, M.T., and Montagna, P. (2018) A simple
756 biomineralization model to explain Li, Mg, and Sr incorporation into aragonitic foraminifera
757 and corals. Earth Plan. Sci. Lett. 481, 20-29.
758 Marchitto, T. M., Bryan, S. P., Curry, W. B., and McCorkle, D. C. (2007) Mg/Ca temperature
759 calibration for the benthic foraminifer *Cibicidoides pachyderma*. Paleoceanography 22,
760 PA1203.
761 Marriott, C.S., Henderson, G.M., Belshaw, N.S. and Tudhope, A.W. (2004a) Temperature
762 dependence of δ7Li, δ44Ca and Li/Ca during growth of calcium carbonate. Earth Plan. Sci.
763 Lett. 222, 615-624.
764 Marriott, C.S., Henderson, G.M., Crompton, R., Staubwasser, M. and Shaw, S. (2004b)
765 Effect of mineralogy, salinity, and temperature on Li/Ca and Li isotope composition of
766 calcium carbonate. Chem. Geol. 212, 5-15.

Martin, S., Charnoz, A. and Gattuso, J.-P. (2013) Photosynthesis, respiration and calcification in the Mediterranean crustose coralline alga Lithophyllum cabiochae (Corallinales, Rhodophyta). European J. Phycol. 48, 163-172.
McConnaughey, T.A. and Falk, R.H. (1991) Calcium-Proton Exchange During Algal Calcification. The Biological Bulletin 180, 185-195.
McConnaughey, T.A. and Whelan, J.F. (1997) Calcification generates protons for nutrient and bicarbonate uptake. Earh-Science Rev. 42, 95-117.
McCulloch, M., Trotter, J., Montagna, P., Falter, J., Dunbar, R., Freiwald, A., Försterra, G., López Correa, M., Maier, C., Rüggeberg, A. and Taviani, M. (2012) Resilience of cold-water scleractinian corals to ocean acidification: Boron isotopic systematics of pH and saturation state up-regulation. Geochim. Cosmochim. Acta 87, 21-34.
Moberly, R. (1968) Composition of magnesian calcites of algae and pelecypods by electron microprobe analysis. Sedimentology 11, 61-82.
Montagna, P., McCulloch, M., Douville, E., López Correa, M., Trotter, J., Rodolfo-Metalpa, R., Dissard, D., Ferrier-Pagès, C., Frank, N., Freiwald, A., Goldstein, S., Mazzoli, C., Reynaud, S., Rüggeberg, A., Russo, S. and Taviani, M. (2014) Li/Mg systematics in scleractinian corals: Calibration of the thermometer. Geochim. Cosmochim. Acta 132, 288-310.
Moore, G.W.K. (2016) The December 2015 North Pole Warming Event and the Increasing Occurrence of Such Events. Sci. Rep. 6, 39084.
Nir, O., Vengosh, A., Harkness, J.S., Dwyer, G.S. and Lahav, O. (2015) Direct measurement of the boron isotope fractionation factor: Reducing the uncertainty in reconstructing ocean paleo-pH. Earth Plan. Sci. Lett. 414, 1-5.
Noireaux, J., Mavromatis, V., Gaillardet, J. Schott, J., Montouillout, V., Louvat, P., Rollion-Bard, C., Neuville, D.R. (2015) Crystallographic control on the boron isotope paleo-pH proxy, Earth Planet. Sci. Lett., 430, pp. 398-407.
Notz, D. and Stroeve, J. (2016) Observed Arctic sea-ice loss directly follows anthropogenic CO2 emission. Science 354, 747-750.
Pauly, M., Kamenos, N.A., Donohue, P. and LeDrew, E. (2015) Coralline algal Mg-O bond strength as a marine pCO_2 proxy. Geology 43, 267-270.
Pelejero, C., Calvo, E., McCulloch, M.T., Marshall, J.F., Gagan, M.K., Lough, J.M. and Opdyke, B.N. (2005) Preindustrial to modern interdecadal variability in coral reef pH. Science 309, 2204-2207.
Pentecost, A. (1978) Calcification and photosynthesis in *Corallina officinalis L*. using the $^{14}CO_2$ method. British Phycol J 13, 383-390.
Popova, E.E., Yool, A., Aksenov, Y., Coward, A.C. and Anderson, T.R. (2014) Regional variability of acidification in the Arctic: a sea of contrasts. Biogeosciences 11, 293-308.
Qi, D., Chen, L., Chen, B., Gao, Z., Zhong, W., Feely, Richard A., Anderson, Leif G., Sun, H., Chen, J., Chen, M., Zhan, L., Zhang, Y. and Cai, W.-J. (2017) Increase in acidifying water in the western Arctic Ocean. Nat. Clim. Change 7, 195.
Rahman, M.A. and Halfar, J. (2014) First evidence of chitin in calcified coralline algae: new insights into the calcification process of *Clathromorphum compactum*. Sci. Rep. 4, 6162.
Rahmstorf, S., Box, J.E., Feulner, G., Mann, M.E., Robinson, A., Rutherford, S. and Schaffernicht, E.J. (2015) Exceptional twentieth-century slowdown in Atlantic Ocean overturning circulation. Nat. Clim. Change 5, 475.
Ries, J.B. (2006). Mg fractionation in crustose coralline algae: Geochemical, biological, and sedimentological implications of secular variation in the Mg/Ca ratio of seawater. Geochim. Cosmochim. Acta 70, 891-900.
Ries, J.B. (2011) Skeletal mineralogy in a high-CO_2 world. J. Exp. Mar. Bio. Ecol. 403, 54-64.

Ries, J.B., Cohen, A.L. and McCorkle, D.C. (2009) Marine calcifiers exhibit mixed responses to CO2-induced ocean acidification. Geology 37, 1131-1134.
Roberts, R.D. (2001) A review of settlement cues for larval abalone (Haliotis spp.). J. Shellfish Res. 20, 571–586.
Roy, R.N., Roy, L.N., Vogel, K.M., Porter-Moore, C., Pearson, T., Good, C.E., Millero, F.J., Campbell, D.M. (1993) The dissociation constants of carbonic acid in seawater at salinities 5 to 45 and temperatures 0 to 45°C. Marine Chemistry 44, 249-267.
Sletten, H.R., Gillikin, D.P., Halfar, J., Andrus, C.F.T. and Guzmán, H.M. (2017) Skeletal growth controls on Mg/Ca and P/Ca ratios in tropical Eastern Pacific rhodoliths (coralline red algae). Chem. Geol. 465, 1-10.
Smith, A.D. and Roth, A.A. (1979) Effect of carbon dioxide concentration on calcification in the red coralline alga Bossiella orbigniana. Mar. Biol. 52, 217-225.
Stanley, S.M., Ries, J.B. and Hardie, L.A. (2002) Low-magnesium calcite produced by coralline algae in seawater of Late Cretaceous composition. Proc. Nat. Ac. Sci. 99, 15323-15326.
Steneck, R.S. (1982) A Limpet-Coralline Alga Association: Adaptations and Defenses Between a Selective Herbivore and its Prey. Ecology 63, 507-522.
Steneck, R.S. (1986) The Ecology of Coralline Algal Crusts: Convergent Patterns and Adaptative Strategies. Annu. Rev. Ecol. Syst. 17, 273-303.
Steneck, R.S. and Martone, P.T. (2007) Calcified algae, in: Denny, M.W., Gaines, S.D. (Eds.), Encyclopedia of Tidepools. Berkeley: University of California Press.
Stewart, J.A., Anagnostou, E. and Foster, G.L. (2016) An improved boron isotope pH proxy calibration for the deep-sea coral *Desmophyllum dianthus* through sub-sampling of fibrous aragonite. Chem. Geol. 447, 148-160.
Sutton, J.N., Liu, Y.-W., Ries, J.B., Guillermic, M., Ponzevera, E. and Eagle, R.A. (2018) $\delta^{11}B$ as monitor of calcification site pH in divergent marine calcifying organisms. Biogeosciences 15, 1447-1467.
Thirumalai, K., Singh, A. and Ramesh, R. (2011) A MATLAB™ code to perform weighted linear regression with (correlated or uncorrelated) errors in bivariate data. Journal of the Geological Society of India 77, 377-380.
Uppstrom, L.R. 1974. The boron/chlorinity ratio of deep-sea water from the Pacific Ocean. Deep Sea Research 21,161−162.
Venn, A., Tambutté, E., Holcomb, M., Allemand, D. and Tambutté, S. (2011) Live tissue imaging shows reef corals elevate pH under their calcifying tissue relative to seawater. PLoS One 6, e20013.
Venn, A.A., Tambutté, E., Holcomb, M., Laurent, J., Allemand, D. and Tambutté, S. (2013) Impact of seawater acidification on pH at the tissue-skeleton interface and calcification in reef corals. Proc. Nat. Ac. Sci. 110, 1634-1639.
Wei, G., McCulloch, M.T., Mortimer, G., Deng, W. and Xie, L. (2009) Evidence for ocean acidification in the Great Barrier Reef of Australia. Geochim. Cosmochim. Acta 73, 2332-2346.
Williams, S., Adey, W., Halfar, J., Kronz, A., Gagnon, P., Bélanger, D., and Nash, M. (2018) Effects of light and temperature on Mg uptake, growth, and calcification in the proxy climate archive. Biogeosci. 15, 5745-5749.
Williams, B., Halfar, J., DeLong, K.L., Hetzinger, S., Steneck, R.S. and Jacob, D.E. (2014) Multi-specimen and multi-site calibration of Aleutian coralline algal Mg/Ca to sea surface temperature. Geochim. Cosmochim. Acta 139, 190-204.
Williams, B., Halfar, J., Steneck, R.S., Wortmann, U.G., Hetzinger, S., Adey, W., Lebednik, P. and Joachimski, M. (2011) Twentieth century $\delta^{13}C$ variability in surface water dissolved

inorganic carbon recorded by coralline algae in the northern North Pacific Ocean and the Bering Sea. Biogeosciences 8, 165-174.
Yang, Q., Dixon, T.H., Myers, P.G., Bonin, J., Chambers, D., van den Broeke, M.R., Ribergaard, M.H. and Mortensen, J. (2016) Recent increases in Arctic freshwater flux affects Labrador Sea convection and Atlantic overturning circulation. Nature Communications 7, 10525.
York, D., Evensen, N.M., Martínez, M.L. and Delgado, J.D.B. (2004) Unified equations for the slope, intercept, and standard errors of the best straight line. American J. Phys. 72, 367-375.
Zeebe, R.E. and Wolf-Gladrow, D. (2001) CO_2 in seawater: Equilibrium, kinetics, isotopes. Elsevier.

Table 1. Culture seawater properties and *C. compactum* skeletal analyses. Note the two grey shadings highlight the samples that are replicates from the same replicate tanks.

Culture seawater								*C. compactum* growth		Chemical analyses and derivations						
Temperature (T)	1 sd T	Salinity	CO_2	pH_{sw}	1 sd pH_{sw}	$\delta^{11}B_{borate}$	1 sd $\delta^{11}B_{borate}$	Change in boyant weight	Linear extension	$\delta^{11}B_{cc}$	2se $\delta^{11}B_{cc}$	pH_{cf}	Li/Ca	B/Ca	Mg/Ca	Mg/Li
(°C)		(psu)	(ppm)	(total scale)		(‰)		(mg/cm^2/day)	(mm)	(‰)			(µmol/mol)	(µmol/mol)	mmol/mol	mol/mmol
8.8	0.4	31.9	3103	7.24	0.05	12.57	0.08	3.57	0.27	25.73	0.15	8.83	58.2	338.7	146.7	2.5
8.9	0.4	31.9	2870	7.26	0.06	12.61	0.10	3.35	0.29	25.52	0.15	8.81	52.9	331.6	131.3	2.5
8.9	0.4	31.9	2897	7.25	0.08	12.60	0.12	3.63	0.23	25.62	0.14	8.82	51.5	371.9	141.7	2.8
8.7	0.5	31.9	846	7.73	0.06	13.90	0.25	3.26	0.24	27.78	0.14	8.96	62.6	391.7	142.3	2.3
8.7	0.5	31.9	839	7.73	0.06	13.92	0.24	5.16	0.18	27.81	0.12	8.96	56.8	376.1	142.4	2.5
8.7	0.5	31.9	801	7.75	0.05	14.00	0.23	2.98	0.14	28.62	0.15	9.02	51.6	423.2	123.1	2.4
8.5	0.4	31.9	480	7.95	0.06	15.07	0.37	3.01	0.26	27.69	0.14	8.96	67.3	325.9	163.3	2.4
8.6	0.4	31.9	469	7.95	0.05	15.13	0.31	3.42	0.21	*28.38*	*0.17*	*9.00*	59.3	419.3	144.4	2.4
8.6	0.4	31.9	469	7.95	0.05	15.13	0.31	3.74	0.22	*28.95*	*0.15*	*9.04*	60.2	382.6	145.4	2.4
8.9	0.4	31.9	335	8.09	0.08	16.20	0.62	3.09	0.25	29.81	0.14	9.09	54.0	356.1	132.7	2.5
8.9	0.4	31.9	353	8.07	0.09	16.03	0.65	3.14	0.33	30.54	0.15	9.15	56.7	404.2	138.0	2.4
8.9	0.4	31.9	360	8.07	0.08	15.97	0.61	2.76	0.20	*30.42*	*0.13*	*9.14*	61.3	427.4	140.5	2.3
8.9	0.4	31.9	360	8.07	0.08	15.97	0.61	3.09	0.20	*30.56*	*0.14*	*9.15*	59.6	414.6	136.6	2.3
6.3	0.7	31.9	3354	7.18	0.08	12.44	0.09	3.34	0.18	24.75	0.12	8.80	56.3	342.5	128.3	2.3
6.2	0.9	31.9	3233	7.21	0.11	12.48	0.13	2.14	0.21	24.36	0.12	8.78	61.6	328.5	136.9	2.2
6.2	0.9	31.9	3174	7.18	0.10	12.45	0.11	2.79	0.12	26.18	0.13	8.89	52.2	325.8	126.9	2.4
6.5	0.8	31.9	812	7.74	0.06	13.83	0.25	3.76	0.18	28.13	0.12	9.01	54.9	386.9	125.5	2.3
6.5	0.8	31.9	879	7.70	0.08	13.70	0.30	4.65	0.30	26.48	0.16	8.91	59.8	323.4	141.1	2.4
6.6	0.8	31.9	1110	7.69	0.12	13.64	0.40	4.62	0.20	26.74	0.14	8.92	66.6	366.3	149.2	2.2
6.5	0.8	32.0	469	7.95	0.06	14.91	0.33	3.93	0.48	27.03	0.11	8.94	60.8	343.8	149.1	2.5
6.4	0.8	32.0	514	7.95	0.05	14.91	0.32	2.64	0.27	26.88	0.14	8.93	76.4	344.8	152.4	2.0
6.4	0.9	32.0	490	7.93	0.08	14.81	0.45	3.07	0.35	26.62	0.16	8.92	76.5	366.7	168.7	2.2
6.4	0.9		490					3.79	0.24				61.7	380.5	131.6	2.1
6.4	0.8	31.9	338	8.09	0.09	15.89	0.65			28.67	0.14	9.05	46.6	321.7	130.8	2.8
6.4	0.8	31.9	323	8.09	0.06	15.93	0.47	2.61	0.21	29.66	0.17	9.12	58.1	400.5	120.5	2.1
6.3	0.8	31.9	342	8.07	0.09	15.74	0.62	3.31	0.14	30.45	0.14	9.17	53.4	421.4	114.9	2.1
12.3	0.6	31.9	3627	7.21	0.09	12.59	0.13			24.92	0.16	8.73	39.4	318.0	131.6	3.3
12.3	0.6	31.9	3168	7.27	0.10	12.70	0.16			25.22	0.26	8.75	39.9	345.0	120.0	3.0
12.3	0.6		3475					4.00	0.18				40.3	326.7	128.9	3.2
12.4	0.4	31.9	936	7.71	0.05	14.03	0.24	3.26	0.30	27.58	0.12	8.90	52.3	376.2	143.7	2.7
12.4	0.4	31.9	872	7.74	0.04	14.16	0.20	4.25	0.17	27.48	0.12	8.89	41.9	342.4	136.3	3.3
12.4	0.4	31.9	901	7.72	0.07	14.11	0.30	3.46	0.16	27.83	0.17	8.92	43.2	352.0	135.6	3.1
12.4	0.3	31.9	514	7.94	0.07	15.36	0.45	2.39	0.17	28.79	0.13	8.98	57.2	406.8	147.1	2.6
12.4	0.3	31.9	486	7.96	0.03	15.48	0.23	4.93	0.43	28.39	0.12	8.95	50.9	349.5	145.1	2.9
12.4	0.3	31.9	497	7.95	0.03	15.44	0.20	3.71	0.17	29.12	0.18	9.00	44.9	363.0	132.8	3.0
12.4	0.3		499					3.15	0.16				41.5	427.7	129.8	3.1
12.5	0.4	31.9	352	8.08	0.05	16.44	0.45	3.13		30.97	0.15	9.13	45.1	371.9	138.3	3.1
12.5	0.4	31.9	377	8.05	0.06	16.21	0.46	3.13		30.33	0.13	9.09	50.9	409.1	150.0	2.9
12.5	0.4	31.9	385	8.04	0.08	16.16	0.60	2.70		30.58	0.11	9.10	38.8	372.6	136.2	3.5

Table 2. Output of multiple linear regressions for identifying covariations. Note: the calibrations were defined using the weighted regression approach (see Methos). Bold font is used for p<<0.05.

		slope	intercept	t value	P value	Multiple R^2
$\delta^{11}B_{cc}$	(‰)		263.1			0.9
$\delta^{11}B_{borate}$	(‰)	1.32		13.7	**7.60E-13**	
Linear extensior	(mm)	-5.79		-3.95	**6E-04**	
Buoyant weight	(mg/cm^2/day)	0.2		1.14	0.27	
Temperature	(^{o}C)	-1E-04		-2E-03	1.00	
stdev-$\delta^{11}B_{cc}$	(‰)					0.4
pH				0.22	0.83	
Temperature	(^{o}C)			-2.5	0.03	
B/Ca			8847.79			0.5
Linear extensior	(mm)	-137.88		-2.29	**0.03**	
Buoyant weight	(mg/cm^2/day)	-6.0		-0.9	0.38	
Temperature	(^{o}C)	-1.43		-0.62	0.53	
pH		69.08		4.38	**2E-04**	
Mg/Ca			113.22			0.3
Linear extensior	(mm)	76.36		3.03	**6E-03**	
Buoyant weight	(mg/cm^2/day)	-0.51		-0.18	0.86	
Temperature	(^{o}C)	0.49		0.53	0.60	
pH		0.74		0.11	0.91	
Li/Ca			31.05			0.6
Linear extensior	(mm)	30.84		2.26	**0.03**	
Buoyant weight	(mg/cm^2/day)	-2.36		-1.54	0.14	
Temperature	(^{o}C)	-2.14		-4.32	**2E-04**	
pH		5.88		1.63	0.12	
Mg/Li			3.02			0.6
Linear extensior	(mm)	-0.03		-0.09	0.9	
Temperature	(^{o}C)	0.11		9.5	**9E-10**	

Figure 1

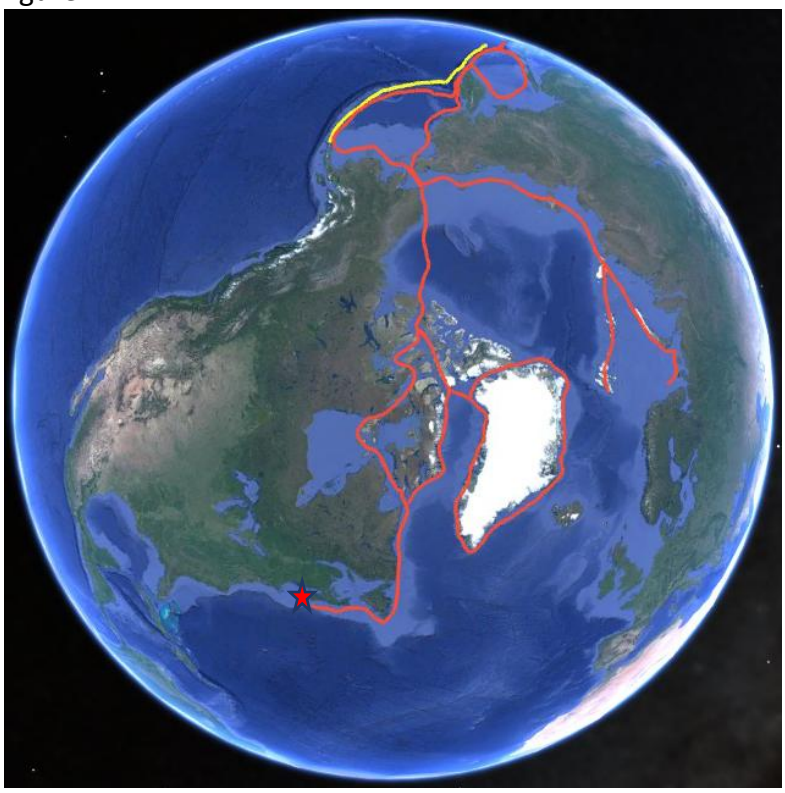

Figure 2

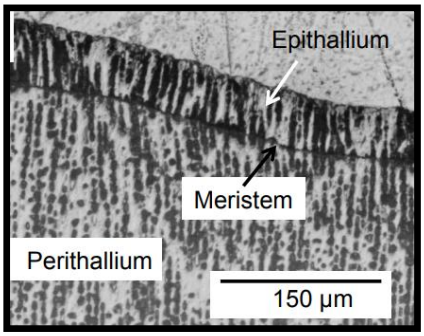

Figure 3

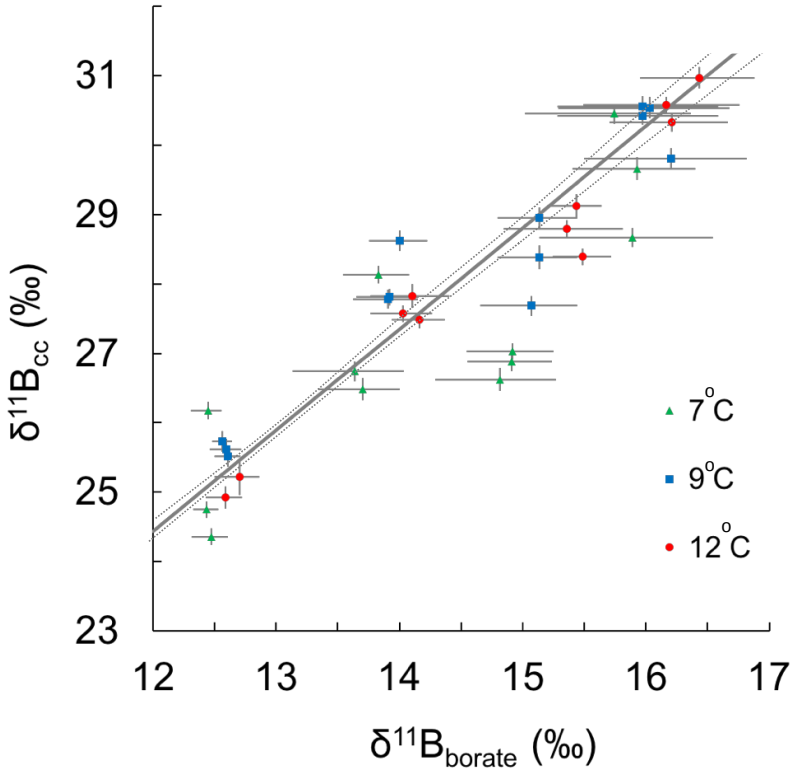

Figure 4

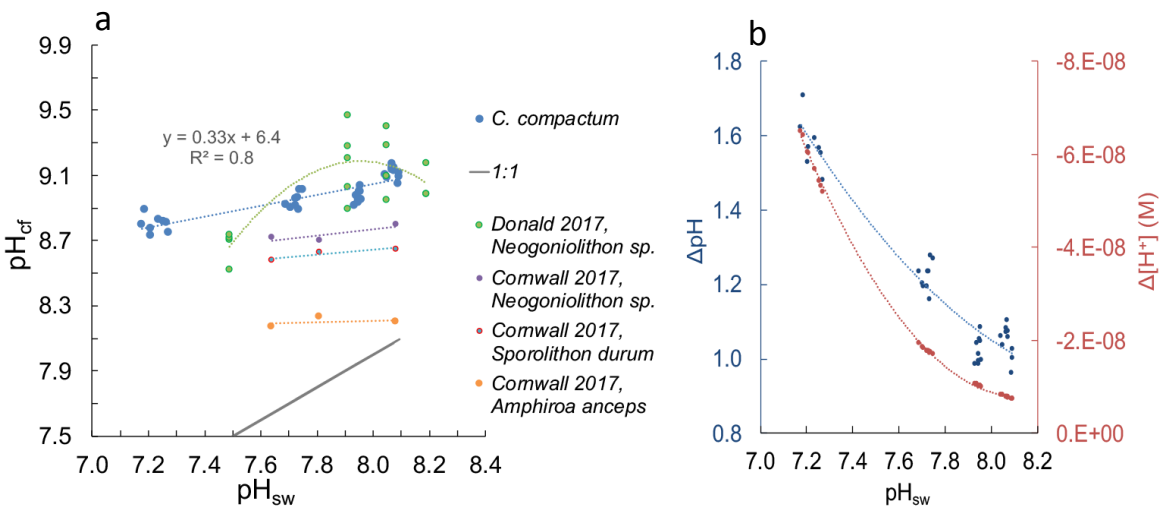
a
9.9
9.5
9.1
8.7
8.3
7.9
7.5
pHcf
y = 0.33x + 6.4
R² = 0.8
7.0 7.2 7.4 7.6 7.8 8.0 8.2 8.4
pHsw
C. compactum
1:1
Donald 2017, Neogoniolithon sp.
Cornwall 2017, Neogoniolithon sp.
Cornwall 2017, Sporolithon durum
Cornwall 2017, Amphiroa anceps
b
1.8
1.6
1.4
1.2
1.0
0.8
ΔpH
-8.E-08
-6.E-08
-4.E-08
-2.E-08
0.E+00
Δ[H+] (M)
7.0 7.2 7.4 7.6 7.8 8.0 8.2
pHsw

Figure 5

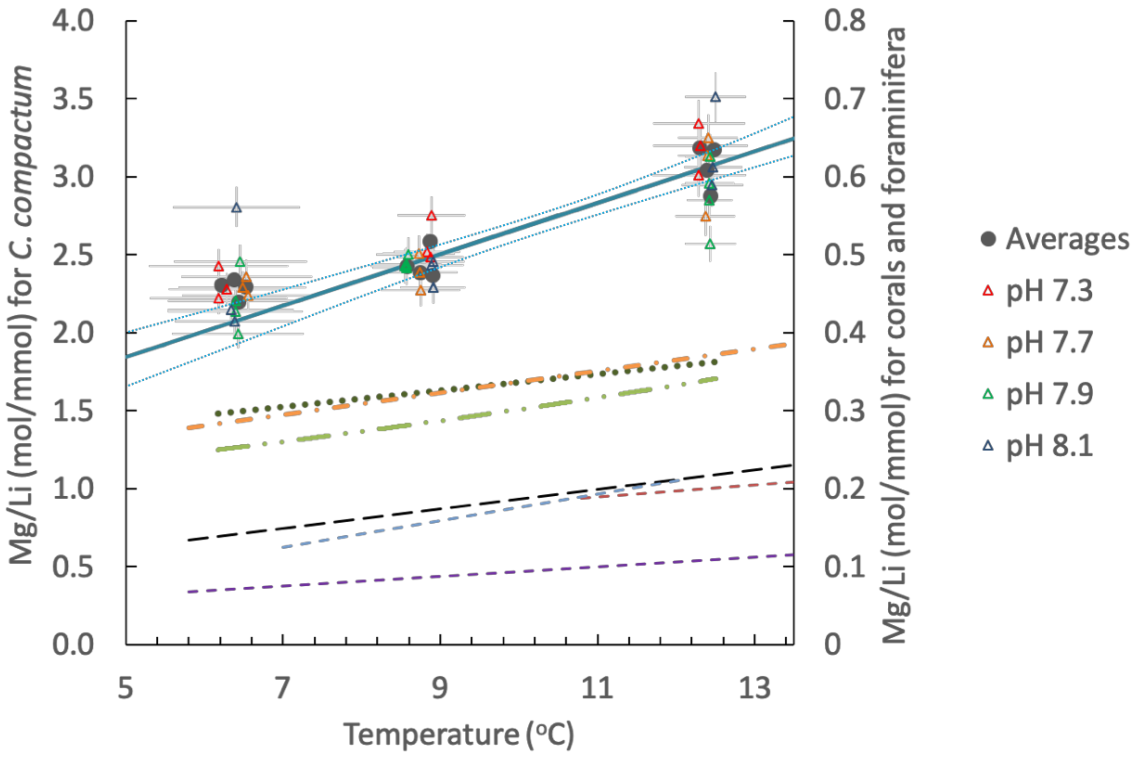
Mg/Li (mol/mmol) for C. compactum
Mg/Li (mol/mmol) for corals and foraminifera
Temperature (°C)
4.0
3.5
3.0
2.5
2.0
1.5
1.0
0.5
0.0
0.8
0.7
0.6
0.5
0.4
0.3
0.2
0.1
0
5
7
9
11
13
Averages
pH 7.3
pH 7.7
pH 7.9
pH 8.1

Electronic supplement

Figure EA1. Coralline algal $\delta^{11}B_{cc}$ plotted against ambient pH_{sw} for the three temperature treatments of the experiment. Purple circles show calculated seawater $\delta^{11}B_{borate}$ for each replicate tank of each experimental treatment.

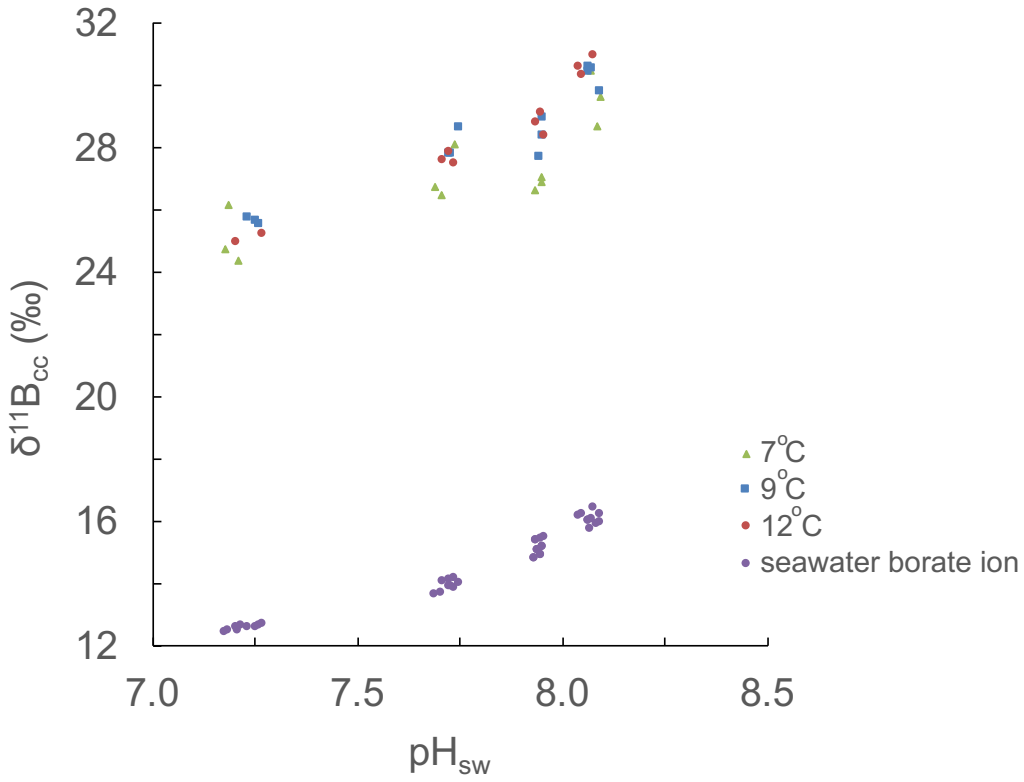

Figure EA2. Seawater pH of experimental treatments reconstructed from coralline algal $\delta^{11}B_{cc}$ and equation 3 (blue circles) and measured seawater pH (orange circles) for all 36 experimental aquaria (12 treatments x 3 replicate tanks). Reconstructed pH has two error bars: blue bars correspond to error in pH arising from the uncertainty of the $\delta^{11}B_{cc}$ measurements and grey bars correspond to error in pH arising from the combination of the uncertainty of the $\delta^{11}B_{cc}$ analyses and the 95% confidence interval of the $\delta^{11}B_{cc}$- $\delta^{11}B_{borate}$ regression. Orange bars correspond to error of measured seawater pH arising from instrumental error and variation in seawater pH throughout the duration of the experiment.

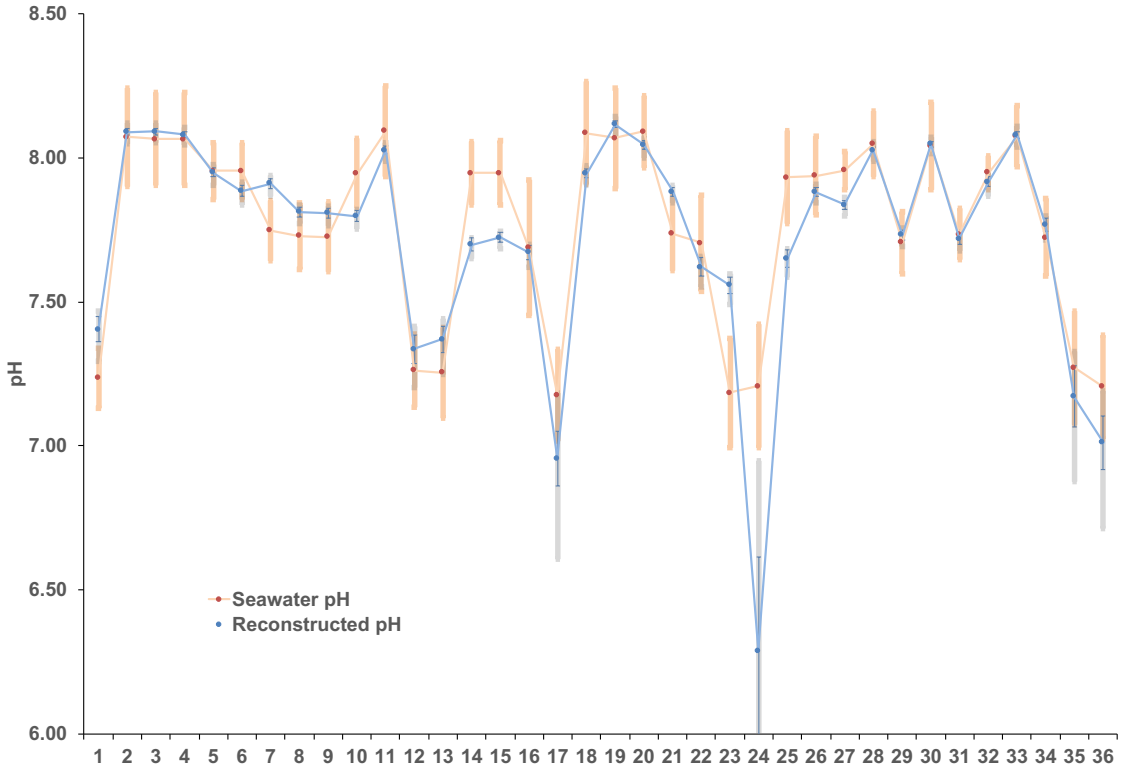

Figure EA3: Relationship between $\delta^{11}B_{cc}$ and B/Ca within skeletons of *C. compactum* specimens investigated in the present study. Linear regression analysis (green line) yields a significant ($p<0.05$) correlation between $\delta^{11}B_{cc}$ and B/Ca. Because of the large variability in B/Ca amongst replicate specimens and relatively low sensitivity of skeletal B/Ca to temperature and pH, this relationship is only used qualitatively. Error bars represent the long-term precision (2σ) of in-house consistency standards as described in Methods.

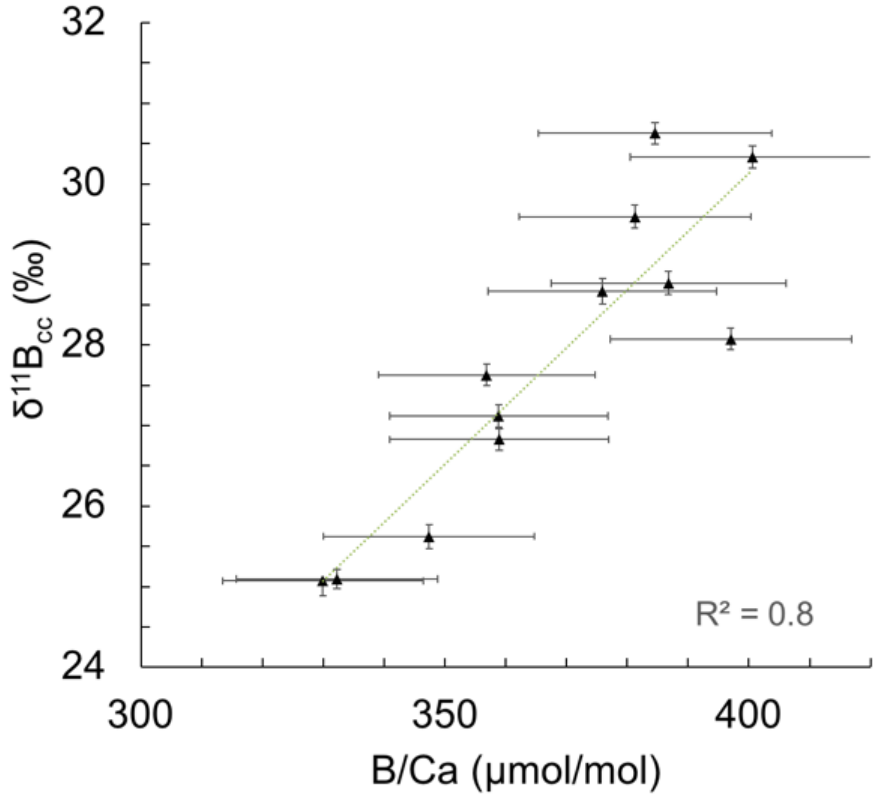

Figure EA4. The Mg/Ca (top panels) and Li/Ca (bottom panels) composition of *C. compactum* skeleton as a function of linear extension rate (left panels) and seawater temperature (right panels). Statistical descriptions of these relationships are provided in Table 2.

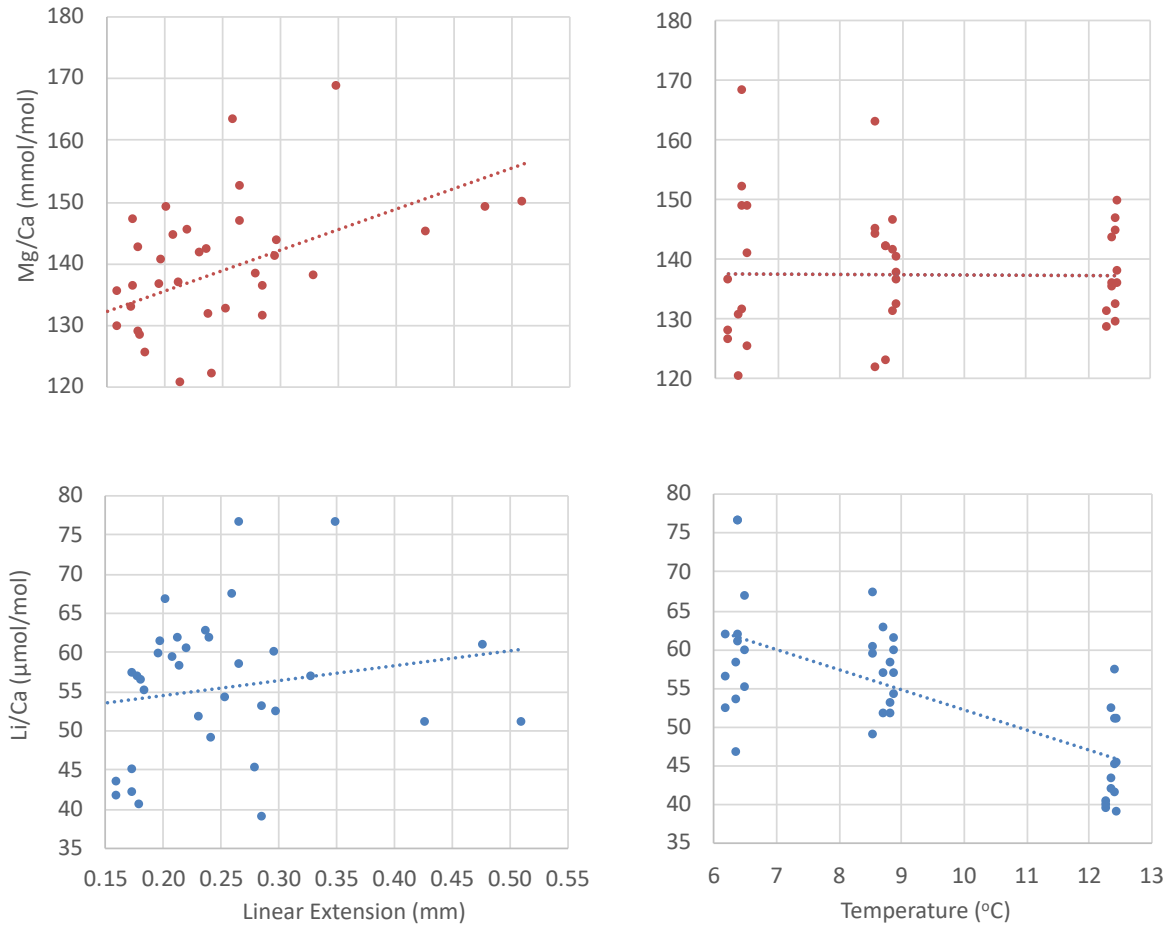

Figure EA5. The relationship between seawater pH (pHsw), linear extension, and calcification rate derived from change in buoyant weight. Data are shown in Table 1.